Iterative Design Reveals Molecular Domain Relationships in Supramolecular Peptide–Drug Conjugates

Matthew J. Sis, Dongping Liu, Isabella Allen, and Matthew J. Webber*

University of Notre Dame, Department of Chemical & Biomolecular Engineering, Notre Dame, IN 46556 USA

*- mwebber@nd.edu

ABSTRACT: Supramolecular peptide-drug conjugates (sPDCs) are prepared by covalent attachment of a drug moiety to a peptide motif programmed for one-dimensional self-assembly, with subsequent physical entanglement of these fibrillar structures enabling formation of nanofibrous hydrogels. This class of prodrug materials presents an attractive platform for mass-efficient and site-specific delivery of therapeutic agents using a discrete single-component molecular design. However, a continued challenge in sPDC development is elucidating relationships between supramolecular interactions in their drug and peptide domains and the resultant impact of these domains on assembly outcomes and material properties. Inclusion of a saturated alkyl segment alongside the prodrug in the hydrophobic domain of sPDCs could relieve some of the necessity for ordered, prodrug-produg interactions. Accordingly, nine sPDCs are prepared here to iterate the design variables of amino acid sequence and hydrophobic prodrug/alkyl block design. All molecules spontaneously formed hydrogels under physiological conditions, indicating a less hindered thermodynamic path to self-assembly relative to previous prodrug-only designs. However, material studies on the supramolecular arrangement, formation, and mechanical properties of the resultant sPDC hydrogels, as well as their drug release profiles, showed complex relationships between the hydrophobic and peptide domains in the formation and function of the resulting assemblies. Together, these results indicate that sPDC material properties are intrinsically linked to holistic molecular design, with coupled contributions from their prodrug and peptide domains in directing properties of the emergent materials.

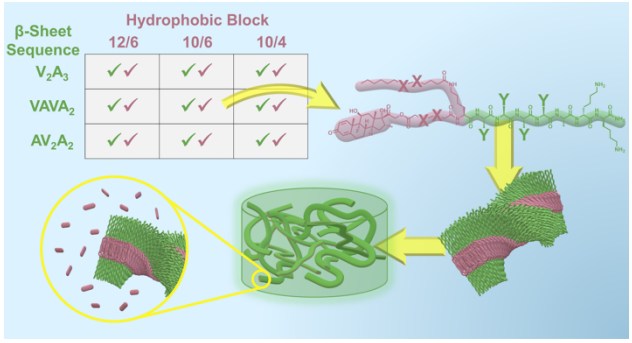

KEYWORDS: Hydrogels; Drug Delivery; Biomaterials; Self-Assembly; Peptide Materials

1. INTRODUCTION

Supramolecular peptide drug conjugates (sPDCs) are a class of drug delivery materials that have shown promising preclinical results in their application to the delivery of a number of small molecule pharmaceutical agents.[1–3] Emerging from robust literature on peptide gelators for drug delivery and tissue engineering,[4–6] sPDCs are most directly inspired by peptide amphiphiles (PA) molecular design.[7] sPDCs typically include a small molecule prodrug as a hydrophobic block attached to a more hydrophilic and (typically) β-sheet-forming peptide to yield an amphiphilic molecular design; the prodrug motif promotes hydrophobic association of the resulting amphiphilic molecules in aqueous environments and contributes to self-assembly of precise nanostructures.[8] The most commonly produced nanoforms are high aspect-ratio one-dimensional nanofibers, which may further engage in physical entanglements to form hydrogels useful as localized drug delivery depots.[9,10] The enhanced therapeutic potential of sPDCs has been increasingly appreciated,[11,12] and exciting recent advances are sPDC formulations that co-deliver both chemotherapies and immunotherapies,[13,14] sPDCs that gel *in situ* on contact with physiological environments,[13–15] and the potential to incorporate bioactive targeting and therapeutic functionalities, such as through integrin or collagen binding peptide sequences,[9,16] and DNA aptamers.[17] Accordingly, sPDC materials constitute a

growing class of peptide-based materials being explored for applications in drug delivery.[18]

A continuing challenge in these materials comes in elucidating and controlling the contributions from prodrug-prodrug interactions in the desolvated nanofiber core to the self-assembly pathway and material properties of the hydrogels. Molecular dynamics simulations have identified the directive forces of prodrug-prodrug interactions as dominant in the early assembly stages of sPDC and other amphiphilic prodrug systems.[19–21] Previous work has also demonstrated the complexity of navigating the sPDC free energy landscape, as well as the drastic changes to the thermodynamics of assembly that result from small topological and chemical changes to the prodrug design.[22] Furthermore, these model systems showed evidence of competitive organizing forces in the prodrug and β-sheet peptide domains, supporting contributions from prodrug modification to the energetics of self-assembly that can interfere with the intended directionality of the fused peptide.[22]

To alleviate prodrug-imposed enthalpic constraints, a promising yet less explored design has included alkylated sPDCs in which a saturated carbon chain is incorporated into the hydrophobic domain of the amphiphile alongside the prodrug.[23,24] In an analogous way to the interactions of lipids and cholesterol in bilayer membranes,[25] inclusion of a saturated alkyl offers conformational and rotational freedom to the prodrug domain in alleviating constraints or kinetic products arising from self-interactions. In one report, an alkylated sPDC showed a lower critical aggregation concentration (CAC), more pronounced β-sheet signatures in circular dichroism (CD), and prolonged drug release compared to prodrug-only sPDCs.[24] This work suggests alkylation of the hydrophobic domain may be a useful strategy to achieve a simpler thermodynamic route to peptide-driven sPDC self-assembly, allowing for the import of peptide design knowledge accumulated from decades of empirical study,[7,26] as well as contemporary machine-driven approaches.[27–29] Also, compared to noncovalent co-formulations of PAs and hydrophobic drugs,[30] alkylated sPDCs maintain the advantages of high and precise drug loading and controlled release *via* labile prodrug linker chemistries.

To test these hypotheses, a set of nine alkylated sPDCs were prepared bearing the anti-inflammatory corticosteroid dexamethasone (DEX) conjugated *via* an ester prodrug linker chemistry. Two variables were independently iterated - the order of valine (V) and alanine (A) residues in the β-sheet segment of the peptide backbone and the relative volume and arrangement of saturated carbon in the hydrophobic domain, achieved by modulating the length of the alkyl segment and prodrug linker. Nanofibrous hydrogels emerged in all cases under physiological conditions, indicating a simpler thermodynamic route to self-assembly versus previously studied prodrug-only DEX sPDCs.[22] Excitingly, all sPDCs also gelled in the presence of sub-physiological saline concentrations, a feature with positive implications for their utility of therapeutic use in the context of injection.[31,32] However, elucidation of trends between design variables and performance in material studies examining peptide and drug domain signatures in CD, the relative stiffness and dynamics of gel formation in oscillatory rheology, and the profiles of drug release *in vitro* were complicated to decipher. Taken together, this study provides evidence for the complex relationship between the prodrug and peptide domain in directing sPDC material properties, and suggests limits of resolution when iteratively tuning these properties *via* rational design.

2. MATERIALS & METHODS

2.1 Materials. Unless otherwise stated, all materials and reagents were purchased from commercial vendors and used as received. Solid phase peptide synthesis reagents, including fluorenylmethyloxycarbonyl-protected (Fmoc) amino acids, Rink Amide AM resin, Oxyma, diisopropylcarbodiimide (DIC), (Benzotriazol-1-yloxy) tripyrrolidinophosphonium hexafluorophosphate (PyBOP), N,N-diisopropylethylamine (DIPEA), hexafluoroisopropanol (HFIP), and trifluoroacetic acid (TFA) were purchased from ChemImpex International Inc. All other chemicals referenced were purchased from commercial vendors through VWR International.

2.2 sPDC Synthesis. Detailed sPDC synthetic protocols are presented in the Online Supporting Information, and the prodrug esterification of DEX is summarized in ***Scheme S1***. UPLC-Abs chromatograms of the pure molecules are presented in ***Figure S1***, and masses of the compounds identified on UPLC-MS (Acquity UPLC-MS, BEH C_{18} column, Waters Technologies Corp.) are presented in ***Table S1***.

2.3 General Gel Preparation. sPDC powders were dissolved at 10 mg/mL in 3/2 v/v acetonitrile (ACN) in deionized (DI) water to disrupt any molecular aggregates that may have formed in the initial sPDC recovery. These solutions were aliquoted to microcentrifuge tubes in 200 μL increments, frozen in liquid nitrogen, and lyophilized. Prior to gel studies, sPDCs were dissolved to 111% of their desired final concentration in DI water. Then, 10% v/v of 10X tris buffered saline (TBS; 100 mM tris, 1 M NaCl) was added to the solution to attain the final sPDC concentration and 1X TBS.

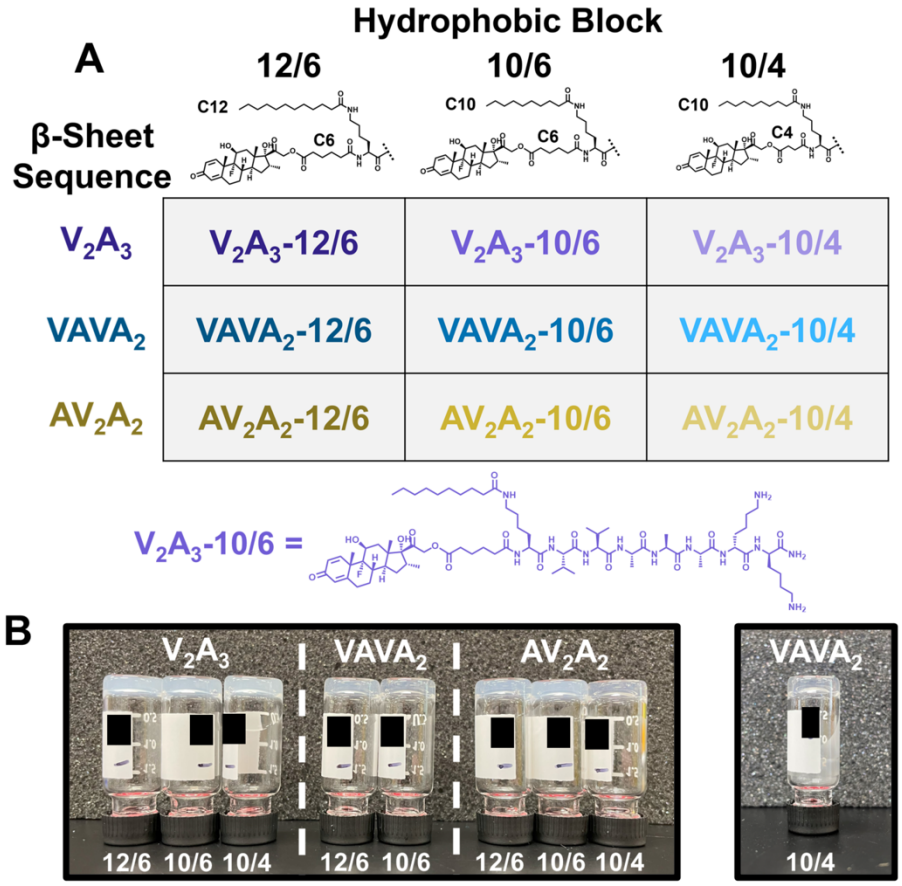

Figure 1. sPDC index and self-supporting sPDC hydrogels. (A) Index describing and coding the names of the nine sPDCs. The order of V and A residues varies across the y-axis while the volume and arrangement of saturated carbon in the alkyl tail and proDEX linker varies across the x-axis. Also, the full molecular structure of **V_2A_3 10/6** is presented. (B, left) All sPDCs except **$VAVA_2$-10/4** form self-supporting hydrogels at 1% (w/v) after overnight incubation at 37°C in 1X TBS (pH 7.4, 10 mM tris, 100 mM NaCl). (B, right) **$VAVA_2$-10/4** forms a self-supporting hydrogel under the same conditions after 96 h of incubation.

2.4 Circular Dichroism (CD). sPDC solutions were prepared at 0.3 mg/mL in DI water or 1X TBS. In the case of 1X TBS samples, sPDCs were diluted to 0.33 mg/mL in DI water before final adjustment with 10% v/v 10X TBS. Spectra of sPDCs bearing hydrophobic block **10/4** were taken 30 mins after dissolution (J-815 CD spectrometer, Jasco) at 25°C in a 1 mm path quartz cuvette (Starna Cells). All sPDC spectra were also collected after 18 h of incubation at room temperature.

2.5 TEM sPDCs solutions were prepared in 1X TBS and incubated for 6 h prior to grid casting. sPDCs bearing peptide sequences **V_2A_3** and **$VAVA_2$** were prepared at 0.3 mg/mL, and those bearing peptide sequence **AV_2A_2** were prepared at 0.1 mg/mL. These samples were deposited onto Formvar/Carbon 200 mesh grids (Ted Pella) and stained with 2% Uranyl Acetate. TEM visualization was performed on Thermo Scientific Talos F200i (S) TEM with an accelerating voltage of 120 kV.

2.6 Rheology. sPDCs were dissolved in DI water at 11.1 mg/mL. 10% v/v 10X TBS was added and mixed, and solutions were pipetted immediately to the lower geometry of the rheometer (TA Instruments HR-2 Discovery hybrid rheometer). The 25 mm stainless steel upper geometry was set to a gap of 250 μm, and the geometries were sealed with a thin layer of silicon oil to prevent sample evaporation. Samples were incubated and manipulated between 25°C and 45°C thermal states, using a ramp rate of 4°C/min to conduct the transitions.

2.7 In Vitro Drug Release. Triplicate samples of each sPDC were dissolved in DI water at 11.1 mg/mL. 0.150 mL of these solutions were transferred to 1.8 mL autosampler vials and mixed with 10% v/v 1X TBS. Samples were incubated at 37°C until self-supporting gels were observed. 1 mL of 1X TBS was added above the gels, and 0.900 mL was exchanged daily to maintain pseudo-infinite sink conditions. Release samples were analyzed by UPLC-Abs using a 10% to 95% gradient of ACN + 0.1% v/v TFA in water + 0.1% v/v TFA (Acquity UPLC-MS, BEH C_{18} column, Waters Technologies Corp.), and DEX content was quantified against a calibration curve of DEX absorbance at 242 nm.

3. RESULTS & DISCUSSION

3.1 Design Rationale & Hydrogelation Survey. To explore the influence of alkyl modification to the sPDC hydrophobic domain on the resultant self-assembly and material outcomes, saturated alkyl segments were incorporated alongside well studied sPDC molecular design elements. Nine sPDCs were produced for comparative study, and their designs and coded names are presented in the index of ***Figure 1A***, as well as a drawing of the full molecular structure of **V_2A_3-10/6** to illustrate the relationship of the different domains being iteratively modified in this work. An N-terminal lysine (K) residue was used as the site of hydrophobic modification, with an ester-linked proDEX conjugated at its α-amine and the alkyl tail conjugated to its ε-amine. K was chosen to afford extra length to the pendant alkyl through its butylamine side chain. Prototype designs suggested that the relationship between alkyl and proDEX linker length may influence material outcomes, and these were accordingly varied to produce hydrophobic blocks with alkyl-to-linker lengths of **12/6**, **10/6**, and **10/4** (***Figure 1A***).

In the peptide backbone, two V and three A residues were incorporated with the intention of driving parallel β-sheet formation along the z-axis of the assembled nanofiber. These amino acids have become routine tools in PA literature, and varying the position and number of V/A residues is known to modulate the β-sheet forming propensity in the resulting peptide assemblies.[33,34] Accordingly, three β-sheet forming peptide backbones were prepared: **V_2A_3**, **$VAVA_2$**, and **AV_2A_2** (***Figure 1A***). Importantly, because the number of V/A residues is the same in every design, all sPDCs with the same hydrophobic block are constitutional isomers. Lastly, two D-lysine (k) residues were added at the hydrophilic C-terminus to afford amphiphilicity to the molecules. Charged amino acids are commonly employed as solubilizing agents in PA-type materials; positively charged Lys residues may furthermore enhance retention in the context of anti-inflammatory delivery to negatively charged cartilaginous tissues,[35] overcoming a key barrier of therapeutic retention at this site.[36] The uncommon D-stereochemistry was selected in anticipation of future *in vivo* applications so as to provide stability to sPDCs against peptidases that often target cationic amino acid sequences.[37]

To screen the sPDCs for evidence of self-assembly, a benchtop hydrogelation survey was conducted wherein all nine sPDCs produced self-supporting hydrogels in the hours to days following solubilization and incubation at 37°C (***Figure 1B***). While sPDC **$VAVA_2$-10/4** took 96 h to become a fully self-supporting hydrogel (***Figure 1B***, *right*), gels emerged in all other sPDCs after overnight incubation (***Figure 1B***, *left*). This result indicates that whatever the complexity, the thermodynamic path of the sPDCs from dissolved powders to supramolecular fibrillar networks is spontaneously traversable under mild conditions. This forms an important distinction from our earlier work, where cycling at elevated temperatures, or extended incubation at high concentration, was required to traverse apparent thermodynamic barriers and achieve hydrogelation.[22] While the gelation survey was conducted at 1% (w/v), sPDC **V_2A_3-12/6** also showed gelation at concentrations as low as 0.2% (w/v), further indicating the reliable self-assembly characteristics of these alkylated sPDC designs (***Figure S2A***).

Another promising result from the preliminary gelation survey was the ability of all sPDCs to assemble upon addition of sub-physiological saline. Classical PA designs utilizing anionic or cationic solubilizing amino acid domains face two major energy barriers in their self-assembly at physiological pH: *i)* charge-charge repulsion among peptide headgroups that inhibits monomer recruitment and growth of peptide fibers, and *ii*) charge-charge repulsion between fiber surfaces, which inhibits physical entanglement and network formation. Typically to overcome these barriers, divalent screening ions complementary to the net charge of the monomers are necessary, such as Ca^{2+} or HPO_4^{2-}.[6,22,38] However, the sPDCs here overcame these repulsive effects through only Debye screening from monovalent Cl^- and Na^+ ions.[39] Further evidence for this is the accelerated gelation of **$VAVA_2$-10/4** by excess NaCl. While gelation in 100 mM NaCl took 96 h (***Figure 1B***, *right*), the same material formed gels in <1 h after the addition of 10% (v/v) 6.1 M NaCl (***Figure S2B***). It is also likely that salt addition aids in gelation through the dehydration of the peptide domain *via* the Hofmeister effect.[39,40] Again looking towards future applications, the ability of sPDCs to gel spontaneously in physiological conditions could provide exciting benefits such as *in situ sol-gel* transition upon injection and extended gel lifetime *in vivo*.

3.2 β-Sheet Propensity & ProDEX Packing. To more closely interrogate the supramolecular features of sPDC assemblies, all molecules were next examined by CD spectroscopy (***Figure 2***). Samples were prepared at 0.3 mg/mL in either or 1X tris-buffered saline (TBS) or deionized (DI) water and aged over 18 h to allow for equilibrated nanostructure formation. Of note, sPDCs with hydrophobic block **10/4** were found to be much less hydrolytically stable, with hydrolysis of between 29% and 56% of the prodrug after 24 h of incubation at 0.3 mg/mL (***Figure S1***). This agrees generally with previous findings of the effects of linker length and other molecular features on the stability of ester prodrugs.[41,42] In light of this, CD spectra of **10/4** sPDCs were also taken when freshly

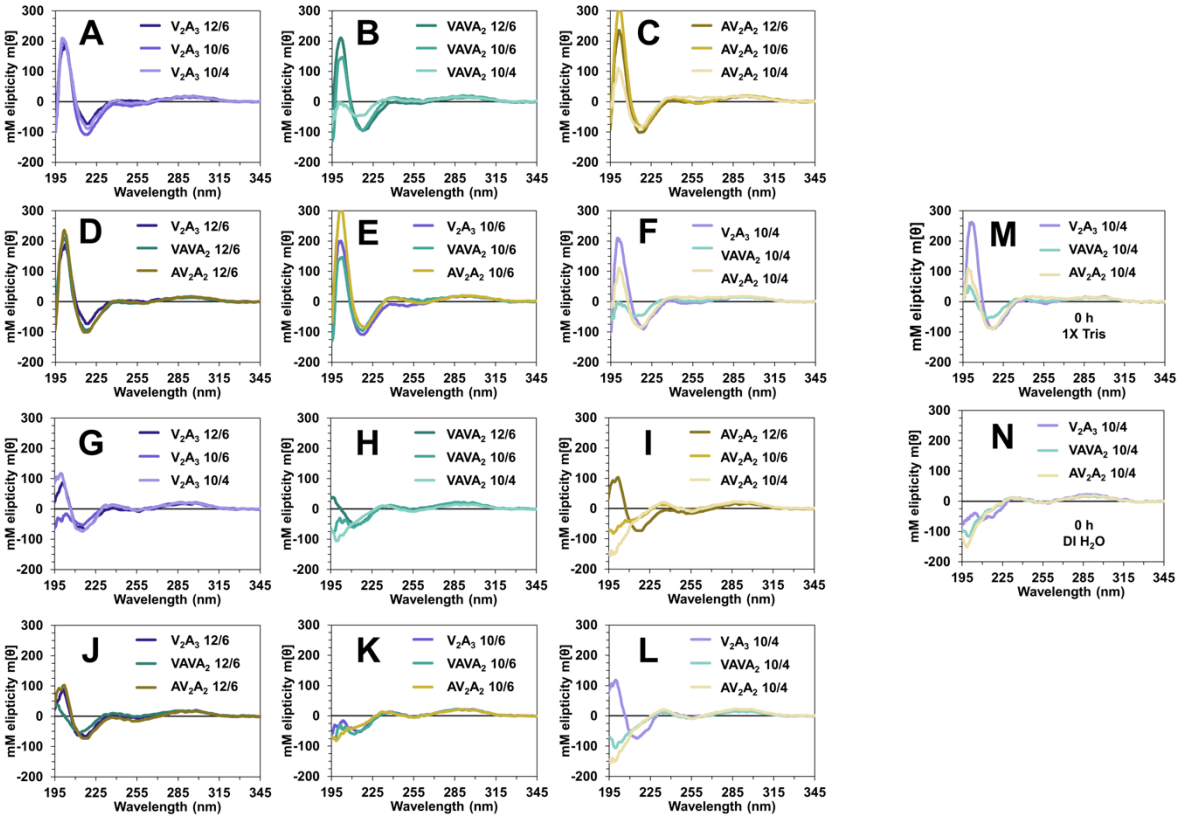

Figure 2 sPDC circular dichroism (CD). CD spectra of sPDCs incubated at 0.3 mg/mL in 1X TBS (A-F) and DI H_2O (G-L) at room temperature for 18 h. A-C and G-I compares a preserved peptide sequence against variable hydrophobic blocks, while the D-F and J-K compares variable peptide sequences against a preserved hydrophobic block. (M,N) Comparison of **10/4** sPDCs at 0 h, 0.3 mg/mL in either 1X TBS or DI H_2O.

dissolved to best capture the supramolecular behavior of intact sPDCs prior to bond rupture and DEX release (***Figure 2M,N***).

Examining the spectra in TBS, all sPDCs except **$VAVA_2$-10/4** show strong parallel β-sheet signatures, represented by their maxima and minima in the far-UV centered at approximately 201 nm and 218 nm, respectively (***Figure 2A-F***). The bathochromic shift in the extrema relative to canonical values for parallel β-sheets indicates some degree of twisting along the fibrillar z-axis, which is typical for materials of the general PA class.[33] While simple peptide systems allow for comparison of the relative effective β-sheet concentration *via* the signal extrema,[33] the β-sheet signal in the sPDCs also overlaps with signal regions arising from molecular CD of the DEX molecule,[22] which may be enhanced by any interactions between DEX chromophores occurring in the core of the assembly. These effects have been noted for other sPDCs bearing more optically active prodrugs.[43] Indeed, relative differences in the spectra from 230 nm to 270 nm indicate differential proDEX packing. In regards to a hypothesis that hydrophobic domain alkylation would relieve the necessity for ordered proDEX interactions, it is apparent that this is only partially the case and the extent of proDex interactions remains design-dependent due to the interplay between organizing forces in hydrophobic and β-sheet domains of the assemblies. Further evidence of this is the precise signal overlap of drug-associated signals in the mid-UV and near-UV when β-sheets are absent (***Figure 2K,N***), indicating that β-sheet formation induces at least some changes to prodrug ordering.

Examining the outlying case of **$VAVA_2$-10/4** (***Figure 2B***), the peptide domain likely exists as a mix of random coil and β-sheet structures, leading to a complex signal in the far-UV. The β-sheet presence may still be interpreted by the minima centered at ~213 nm, with hypsochromic shift and distortion of the magnitude caused by an overlapping random coil signal. Also, the **$VAVA_2$-10/4** spectra in 1X TBS at 0 h (***Figure 2M***) presents both of the far UV-signals associated with β-sheet formation: a maxima centered at 200 nm and minima centered at 214 nm. This result indicates a stronger β-sheet propensity prior to significant DEX hydrolysis, likely due to the increased anchoring effect of more hydrophobic mass on the constituent monomers within the assembly.

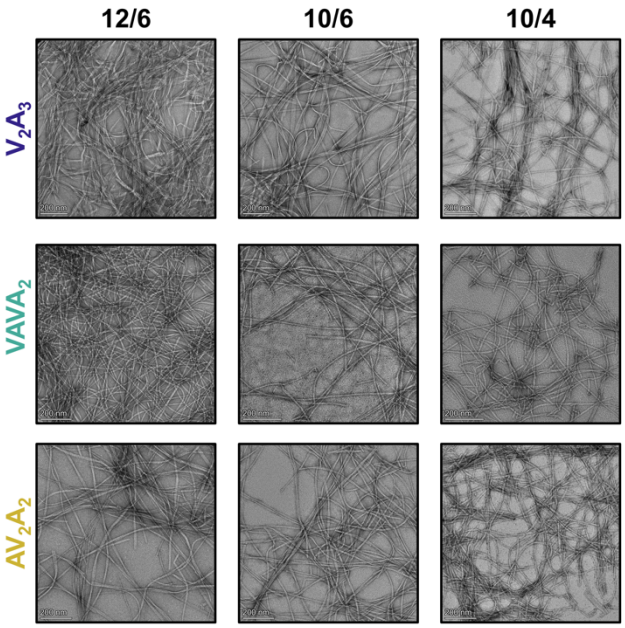

Figure 3. sPDC transmission electron microscopy (TEM). All samples were prepared in 1X TBS (pH 7.4, 10 mM tris, 100 mM NaCl) and incubated for ~6 h prior to grid preparation. **V_2A_3** and **$VAVA_2$** series sPDCs were prepared at 0.3 mg/mL while **AV_2A_2** series peptides were prepared at 0.1 mg/mL to optimize nanofiber density in imaging.

More information regarding relative β-sheet propensities of sPDCs can be found by examining the DI water spectra (***Figure 2G-L***). As discussed, charge-charge repulsion among the cationic primary amines of the hydrophilic domain are an entropic barrier to the association of monomers necessary to form β-sheets and nanofibers. However, five of the nine sPDCs are able to overcome this repulsion, even in the absence of screening salt. In particular, all **V_2A_3** sPDCs show a far-UV β-sheet minima (***Figure 2G***) as well as all designs with the **12/6** hydrophobic block (***Figure 2J***). Taken together, these sPDCs likely experience a balance of cohesive forces from the specific V/A sequence as well as the relief of enthalpic prodrug-prodrug constraints in the hydrophobic domain *via* alkylation. In correlating PA systems, β-sheet propensity generally increases when more V residues are proximate to the hydrophobic block,[33] as is the case for **V_2A_3**. Considering the hydrophobic domain, the **C6** linker provides the most significant rotational freedom to the proDEX motif, while the **C12** alkyl may best match the length of the linker to optimize entropic interactions between tails and prodrug. Finally, the lower intensities of *β*-sheet signals in the DI water experiments relative to those in 1X TBS indicate that while β-sheet formation in pure aqueous environments is possible, it is enhanced by the presence of screening salts.

3.3 sPDC Nanofiber Morphology. To assess the impact of molecular design on nanofiber morphology, the different sPDC samples were imaged with transmission electron microscopy (TEM) (***Figure 3***). Solutions were prepared in 1X TBS and incubated at room temperature for approximately 6 h prior to dropping onto TEM grids, with subsequent negative staining by uranyl acetate. In all nine designs, sPDCs formed one-dimensional nanostructures with flat, ribbon-like morphology having regular intervals of twisting and a high degree of entanglement. Subtle differences were apparent between the peptide sequences, with **$VAVA_2$** backbones appearing to form the thinnest fibers when comparing the width of the flat lamelle, and also appearing to have the least twists. The variance is consistent with other studies on constitutionally isomeric PAs,[44,45] and demonstrates nanofiber morphology is intrinsically linked with molecular design. Generally, morphology appeared well-preserved for a given peptide sequence, regardless of the hydrophobic block design.

3.4 Gel Formation and Kinetics. With knowledge of sPDC behavior at the molecular and nanoscale developed from CD and TEM, it was next desirable to assess macroscopic hydrogel properties, including mechanical properties and kinetics of hydrogelation. Accordingly, sPDC gels were formed *in situ* on the stage of an oscillatory rheometer (***Figure 4***). This not only allowed for assessment of the final state of the materials, but provided qualitative information about the dynamic period of fibrous network formation, as probed by thermal cycling of the samples between 25°C and 45°C. All sPDCs formed hydrogels, as defined by a storage modulus (G′) greater than the loss modulus (G′′), supporting the earlier gross inspection of the samples by vial inversion. Notably, while sPDC **$VAVA_2$-10/4** meets the technical definition of a hydrogel, it is extremely soft, with peak G′ in the tens of Pascals (Pa) **(*Figure 4F*)**. As **$VAVA_2$-10/4** takes 4 d to become fully self-supporting (***Figure 1B***, *right*) it is reasonable to assume stiffer gels may be obtained by extremely long incubation. Also, gelation is likely to be additionally complicated in all **10/4** bearing sPDCs due to the hydrolysis of some proDEX during the assembly process. Comparing the three hydrophobic block designs, sPDCs bearing **10/4** uniformly had the lowest G′ at the end of the experiment. This was most drastic in the case of **$VAVA_2$** sPDCs (***Figure 4D-F***), where **$VAVA_2$-10/4** was over 300-fold softer than the stiffest gel, **$VAVA_2$-10/6.** Similarly, in **AV_2A_2** sPDCs (***Figure 4G-I***), **AV_2A_2-10/4** was 100-fold softer than **AV_2A_2-12/6** at the end of the experiment. When comparing the

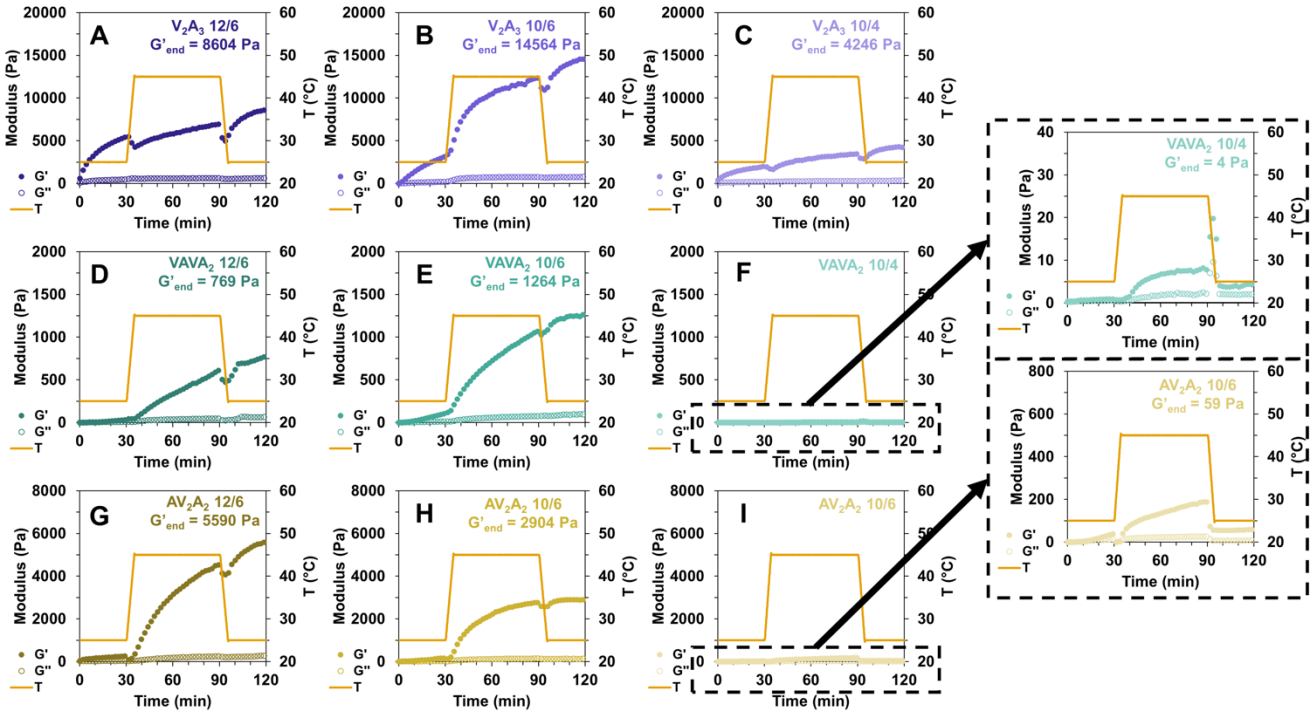

Figure 4 sPDC gel formation *in situ* on oscillatory rheometer. sPDC solutions were freshly prepared at 1% w/v in 1X TBS (pH 7.4, 10 mM tris, 100 mM NaCl). Samples were manipulated at 0.5% strain, 10 rad/s for the duration of the thermal cycle.

differences in stiffness attained by the **12/6** and **10/6** hydrophobic block designs, the results were much more similar within each peptide design. For peptide backbones **V$_2$A$_3$** (***Figure 4A,B***), **VAVA$_2$** (***Figure 4D,E***), and **AV$_2$A$_2$** (***Figure 4G,H***), the final G′ attained by gels bearing hydrophobic blocks **12/6** and **10/6** were within 2-fold of each other. While intermolecular assembly phenomenon cannot be isolated from differences in the fibrous network effects in this technique, it is clear that hydrophobic block design had the most significant impact on hydrogel mechanical properties.

In addition to end-state comparison of G′, it was also useful to consider the dynamic period of network formation and the response of the materials to thermal cycling. Generally, thermal energy accelerates the kinetic steps in supramolecular fiber assembly, but also weakens enthalpic interactions, such as hydrogen bonding within peptide secondary structures.[22,46] Thus, the bulk behavior of the sPDC gels during the period at 45°C reflects a qualitative sum of an accelerated progress through thermodynamic energy barriers alongside a secondary structure "melting" phenomenon. While rheology is a bulk technique and effects at the nanoscopic and bulk network level are not fully separable, these competing phenomena may still be broadly identified, especially in extreme cases. For example, considering **V$_2$A$_3$-12/6** (***Figure 4A***) it is notable that the gel develops a robust G′ spontaneously at 25°C, softens initially upon heating, and only stiffens moderately by the end of the warm phase. This suggests that **V$_2$A$_3$-12/6** faces a relatively low energy barrier towards fiber formation and the assembly is largely complete prior to heating, meaning that β-sheet melting is the dominant process reflected in the softening during the warm phase. Conversely, all other **12/6** and **10/6** hydrophobic block sPDCs showed little softening during the thermal ramp to 45°C and significant growth in G′ during the warm phase (***Figure 4B,D,E,G,H***). While gelation is spontaneous at lower temperature, it is clear that fiber growth is kinetically limited, and acceleration of assembly during the warm phase outweighs β-sheet instability as the determinant factor in enhancing the final G′ values of the hydrogels.

Also notable in all sPDCs is their response to cooling to 25°C at the end of the thermal cycle. sPDCs with hydrophobic block **12/6**, **10/6**, and **V$_2$A$_3$-10/4** had brief reduction in G′ upon initiation of the thermal cooling ramp before returning to an increased trajectory during 25°C incubation (***Figure 4A-C,D,E,G,H***). This is to be expected, as sPDC β-sheets become more stable at cooler temperatures and impart fiber elasticity. Conversely, sPDCs **VAVA$_2$-10/4** and **AV$_2$A$_2$-10/4** stiffen instantaneously during the cooling ramp before developing a softer equilibrium at 25°C (***Figure 4F,I***). This is similar to the behavior demonstrated by prodrug-only DEX sPDCs, in which the cooling-softening effect was

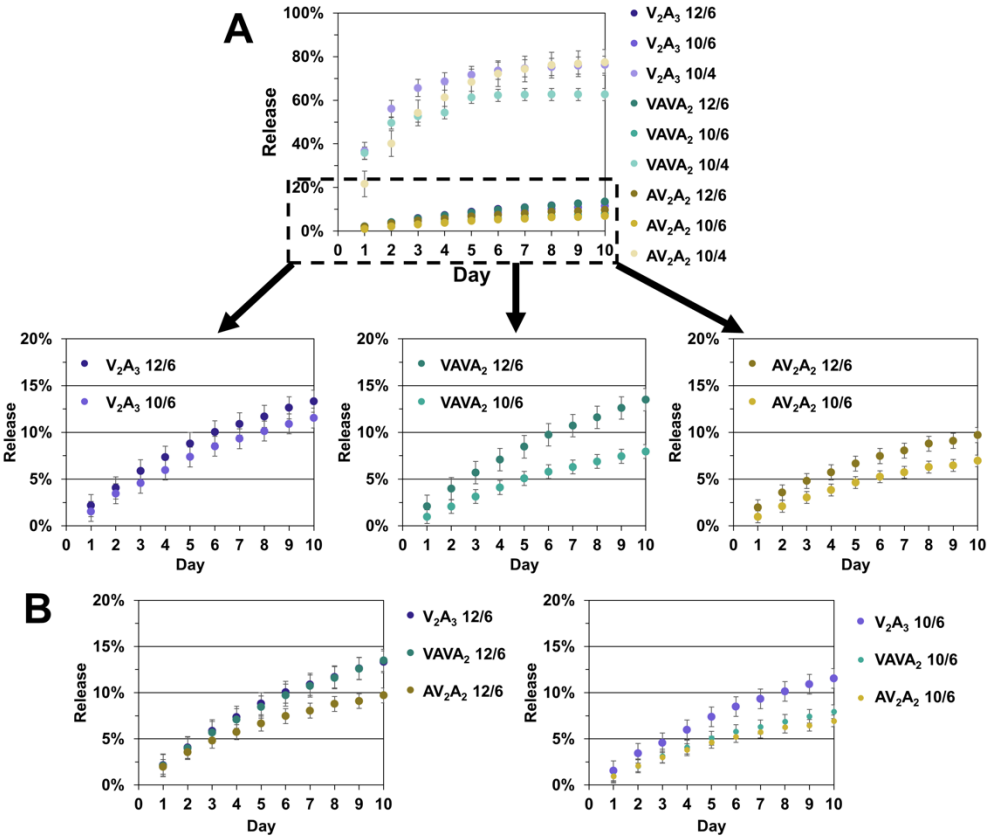

Figure 5 *In* vitro sPDC drug release. DEX release from 1% w/v sPDC gels into bulk 1X TBS over 10 days. (A, top) All **10/4** sPDCs hydrolyze and rapidly release drug. (A, bottom) Release from **12/6** and **10/6** sPDCs, comparing a preserved peptide design against variable hydrophobic block. (B) Release from **12/6** and **10/6** sPDCs, comparing variable peptide designs against a preserved hydrophobic block.

attributed to enthalpic constraints (e.g., hydrogen bonding, planar stacking, and π-π interactions in the prodrug domain) imposed by preferred DEX ordering, which in turn limited β-sheet hydrogen bonding.[22] Considering **$VAVA_2$-10/4** and **AV_2A_2-10/4**, the short C4 linker may impose conformational constraints on the proDEX such that it prefers ordered self interactions among adjacent monomers. While **V_2A_3-10/4** does not show these effects (***Figure 4C***), this specific arrangement of V/A residues may create an overall greater β-sheet propensity, thereby overcoming any proDEX ordering as the predominant factor dictating the G′ at the end of the thermal cycle.

3.5 sPDC Drug Release. As a final evaluation of functionally relevant sPDC performance, drug release kinetics were studied by incubating hydrogels against bulk buffer for 10 d (***Figure 5***). Drug concentration was quantified *via* ultra high performance liquid chromatography (UPLC). For all sPDCs, free DEX was the only drug product released at quantifiable concentrations. It is unknown if hydrolysis occurs within the hydrogel network or from sPDC monomers or aggregates exchanging between nanofibers and the bulk buffer. Interestingly, **$VAVA_2$-10/4** hydrogel samples incubated for > 50 d without buffer immersion showed crystallization of the free hydrolyzed DEX within the gel network (***Figure S2C***), suggesting the presence of a bulk diluent is not required to drive prodrug rupture and release.

In agreement with earlier observations of rapid DEX hydrolysis in the **10/4** sPDCs, these gels showed fast release, with 22% to 37% of DEX released in one day, and up to 78% released by the end of the study (***Figure 5A***). Though DEX hydrolysis from **10/4** sPDCs was previously shown to be rapid in dilute concentrations of suspended nanomaterials (***Figure S1***), it is notable that this still tends to occur in the 1% w/v gel. Accordingly, this finding suggests the possibility of interfacial organization of nanofibers that exposes the C4 linker to the aqueous environment, and accordingly nanofiber assembly and physical entanglement/gelation offers limited protective effect for this shorter linker. Interestingly, a hydrogel remains in all **10/4** samples at the conclusion of the study, though **AV_2A_2-10/4** was no longer fully self supporting (***Figure S2D***). It is suspected that following ester hydrolysis drug release, the DEX-free peptide still

constitutes at least a fraction of the remaining hydrogel due to its alkyl tail sustaining cohesion and self-assembly. Moreover, the presence of this DEX-free cleaved product within assemblies may even offer hydrolytic protection for remaining proDEX conjugates.

In contrast, all **12/6** and **10/6** sPDCs showed much slower drug release, between 8% and 14% over 10 d (***Figure 5A***). It was especially surprising that in every peptide design, **12/6** sPDCs released DEX more quickly than **10/6** sPDCs. Another interesting result was that release rates generally decreased as V residues moved away from the hydrophobic domain. For hydrophobic block **12/6**, $\mathbf{AV_2A_2}$ had a noticeably lower rate of release relative to $\mathbf{VAVA_2}$ and $\mathbf{V_2A_3}$ (***Figure 5B***, *left*). For hydrophobic block **10/6**, both sPDCs $\mathbf{AV_2A_2}$ and $\mathbf{VAVA_2}$ were similar, with release rates that were noticeably reduced compared to sPDC $\mathbf{V_2A_3}$ (***Figure 5B***, *right*). Taken together, these results show that conventional PA design principles relating release rate to hydrophobic mass and V/A driven β-sheet propensity cannot be directly translated to sPDCs. Instead, release rates emerge from holistic molecular design.

3.6 Implications on Rational sPDC Design. Reviewing the evidence gathered on the nine sPDC assemblies at the molecular, microscopic, and macroscopic scale, it is clear that material properties emerge from complex relationships between the various supramolecular domains. First considering the hydrophobic block, other design factors are relevant beyond total hydrophobic mass. The comparative lengths of the alkyl to proDEX linker, the rotational freedom of proDEX, and the hydrolytic stability of the ester linker all produce effects which are manifest when comparing preserved peptide designs. Of the three hydrophobic blocks studied, **10/6** appears to provide the most cohesive benefits to the assemblies, providing the lowest levels of drug release across peptide designs (***Figure 5A***). Another important finding is the relative instability of the ester linker in **10/4** sPDCs; rapid release would therefore not be well-aligned with the long-term use of localized anti-inflammatory delivery. This highlights the importance of selecting prodrug chemistries with appropriate kinetics for disease targets, as well as contributions from molecular-scale packing that may render internal hydrolytic chemistries exposed to the bulk aqueous environment, even in amphiphilic sPDC designs. Further study on solvent dynamics as a function of linker position could help to elucidate such effects.[47]

Regarding the peptide motif, the performance of the three sPDC peptide designs were often counterintuitive. By progressively moving V residues away from the hydrophobic domain, the design intent was to reduce β-sheet propensity and, in turn, reduce supramolecular cohesion, leading to softer gels with faster drug release rates. However, this trend did not emerge in gel stiffness, and release rates showed an inverse correlation with V-to-core proximity. It could be that peptide designs yielding less ordered β-sheets manifest longer and more flexible fibers, which on the whole allow for less interfacial contact between proDEX and water, slowing drug release. Further considering peptide design, an unaccounted factor was the supramolecular role of the *N*-terminal K residue used for hydrophobic derivatization. Its amide group and side chain topology, its propensity to participate in peptide secondary structure formation, and its role relative to the other hydrophobic residues is unclear. This speaks generally to the complex relationship between transition regions between the prodrug and peptide in sPDCs, which has previously been explored and optimized on a case-by-case basis,[24] but for which generalizable designs have not emerged.

Finally, beyond the scope of this work but worthy of future study is the dynamic period of sPDC fiber assembly, and how kinetics and mechanisms of assembly influence material outcomes. While all sPDCs studied here achieved transition between binary states—solubilized sPDC monomers to assembled nanofibrous hydrogels—the full complexity of transient intermediates was not captured. For example, sPDC $\mathbf{V_2A_3}$**-12/6** assembled quickly as evidenced in kinetic rheology studies, and achieved the largest G′ of any sPDC after 30 mins of 25°C incubation (***Figure 4***). However, this rapid assembly may represent a kinetically trapped state, and a more idealized thermodynamic product with different material properties could be attainable. Assembly pathway complexity and kinetics are increasingly appreciated in the supramolecular literature,[48–50] and deeper study of these phenomena are sure to aid in the development of functional sPDC materials.

4. CONCLUSIONS

Herein, a set of nine sPDCs was prepared, varying hydrophobic block and peptide backbone design, to study the effects of these design features on nano and macroscale material properties relevant to drug delivery applications. All sPDCs achieved the design goal of assembly and *sol-gel* transition under physiological temperature, pH, and ionic strength. The materials broke from the initial expectations motivating the choice of explored variables, indicating that the material properties were emergent from holistic molecular design rather than the choice of discrete molecular domains. These findings support ongoing study of the factors influencing sPDC assembly, towards the development of simple, predictable, and generalizable assembly architectures.

ASSOCIATED CONTENT

Supporting Information

The Supporting Information is available free of charge on the ACS Publications website.

Detailed Synthetic methods; UPLC-MS results; Gelation Studies (.PDF)

AUTHOR INFORMATION

Corresponding Author

* mwebber@nd.edu

Notes

The authors declare no competing financial interests.

ACKNOWLEDGMENT

MJW gratefully acknowledges funding support for this work from the National Science Foundation CAREER award (BMAT, 1944875). We are also grateful to the NDEnergy Materials Characterization Facility for use of the TA Instruments HR-2 Discovery Hybrid rheometer, the Notre Dame Biophysics Instrumentation Core Facility for use of the Jasco J-815 CD spectrophotometer, and the Notre Dame Integrated Imaging Facility for use of the Thermo Scientific Talos F200i (S) TEM.

REFERENCES

(1) Lin, R.; Cheetham, A. G.; Zhang, P.; Lin, Y.-A.; Cui, H. Supramolecular Filaments Containing a Fixed 41% Paclitaxel Loading. *Chem. Commun.* **2013**, *49* (43), 4968–4970.

(2) Lu, P.; Leslie, F.; Wang, H.; Sodhi, A.; Choi, C.-Y.; Pekosz, A.; Cui, H.; Jia, H. Discovery, Validation, and Prodrug Design of an ACE2 Activator for Treating Bacterial Infection-Induced Lung Inflammation. *J. Control. Release* **2023**, *364*, 1–11.

(3) Wang, H.; Monroe, M.; Leslie, F.; Flexner, C.; Cui, H. Supramolecular Nanomedicines through Rational Design of Self-Assembling Prodrugs. *Trends Pharmacol. Sci.* **2022**, *43* (6), 510–521.

(4) Zhang, Z.; Ai, S.; Yang, Z.; Li, X. Peptide-Based Supramolecular Hydrogels for Local Drug Delivery. *Adv. Drug Deliv. Rev.* **2021**, *174*, 482–503.

(5) Yan, C.; Pochan, D. J. Rheological Properties of Peptide-Based Hydrogels for Biomedical and Other Applications. *Chem. Soc. Rev.* **2010**, *39* (9), 3528–3540.

(6) Webber, M. J.; Matson, J. B.; Tamboli, V. K.; Stupp, S. I. Controlled Release of Dexamethasone from Peptide Nanofiber Gels to Modulate Inflammatory Response. *Biomaterials* **2012**, *33* (28), 6823–6832.

(7) Cui, H.; Webber, M. J.; Stupp, S. I. Self-Assembly of Peptide Amphiphiles: From Molecules to Nanostructures to Biomaterials. *Biopolymers* **2010**, *94* (1), 1–18.

(8) Wang, Y.; Cheetham, A. G.; Angacian, G.; Su, H.; Xie, L.; Cui, H. Peptide–drug Conjugates as Effective Prodrug Strategies for Targeted Delivery. *Adv. Drug Deliv. Rev.* **2017**, *110-111*, 112–126.

(9) Wang, F.; Su, H.; Lin, R.; Chakroun, R. W.; Monroe, M. K.; Wang, Z.; Porter, M.; Cui, H. Supramolecular Tubustecan Hydrogel as Chemotherapeutic Carrier to Improve Tumor Penetration and Local Treatment Efficacy. *ACS Nano* **2020**, *14* (8), 10083–10094.

(10) Webber, M. J.; Langer, R. Drug Delivery by Supramolecular Design. *Chem. Soc. Rev.* **2017**, *46* (21), 6600–6620.

(11) Wang, Z.; Luo, H.; Wang, H.; Xiao, M.; Jia, H.; Ren, C.; Liu, J. Peptide-based Supramolecular Therapeutics for Fighting Major Diseases. *Adv. Funct. Mater.* **2024**. 2314492. https://doi.org/10.1002/adfm.202314492.

(12) Qiao, Y.; Xu, B. Peptide Assemblies for Cancer Therapy. *ChemMedChem* **2023**, *18* (17), e202300258.

(13) Wang, F.; Xu, D.; Su, H.; Zhang, W.; Sun, X.; Monroe, M. K.; Chakroun, R. W.; Wang, Z.; Dai, W.; Oh, R.; Wang, H.; Fan, Q.; Wan, F.; Cui, H. Supramolecular Prodrug Hydrogelator as an Immune Booster for Checkpoint Blocker-Based Immunotherapy. *Sci Adv* **2020**, *6* (18), eaaz8985.

(14) Wang, F.; Huang, Q.; Su, H.; Sun, M.; Wang, Z.; Chen, Z.; Zheng, M.; Chakroun, R. W.; Monroe, M. K.; Chen, D.; Wang, Z.; Gorelick, N.; Serra, R.; Wang, H.; Guan, Y.; Suk, J. S.; Tyler, B.; Brem, H.; Hanes, J.; Cui, H. Self-Assembling Paclitaxel-Mediated Stimulation of Tumor-Associated Macrophages for Postoperative Treatment of Glioblastoma. *Proc. Natl. Acad. Sci. U. S. A.* **2023**, *120* (18), e2204621120.

(15) Wang, F.; Su, H.; Xu, D.; Monroe, M. K.; Anderson, C. F.; Zhang, W.; Oh, R.; Wang, Z.; Sun, X.; Wang, H.; Wan, F.; Cui, H. Therapeutic Supramolecular Tubustecan Hydrogel Combined with Checkpoint Inhibitor Elicits Immunity to Combat Cancer. *Biomaterials* **2021**, *279*, 121182.

(16) Anderson, C. F.; Chakroun, R. W.; Grimmett, M. E.; Domalewski, C. J.; Wang, F.; Cui, H. Collagen-Binding Peptide-Enabled Supramolecular Hydrogel Design for Improved Organ Adhesion and Sprayable Therapeutic Delivery. *Nano Lett.* **2022**, *22* (10), 4182–4191.

(17) Li, Y.; Liang, X.; Shen, C.; Deng, K.; Zeng, Z.; Guo, B.; Xu, X. Bio-Responsive Macromolecular Drug and Small-Molecular Drug Conjugates: Nanoparticulate Prodrugs for Tumor Microenvironment Heterogeneity Management and Therapeutic Response Enhancement. *Small* **2023**, *19* (39), e2301656.

(18) Sis, M. J.; Webber, M. J. Drug Delivery with Designed Peptide Assemblies. *Trends Pharmacol. Sci.* **2019**, *40* (10), 747–762.

(19) Kang, M.; Zhang, P.; Cui, H.; Loverde, S. M. - Stacking Mediated Chirality in Functional Supramolecular Filaments. *Macromolecules* **2016**, *49* (3), 994–1001.

(20) Manandhar, A.; Chakraborty, K.; Tang, P. K.; Kang, M.;

Zhang, P.; Cui, H.; Loverde, S. M. Rational Coarse-Grained Molecular Dynamics Simulations of Supramolecular Anticancer Nanotubes. *J. Phys. Chem. B* **2019**, *123* (50), 10582–10593.

(21) Tang, P. K.; Khatua, P.; Carnevale, V.; Loverde, S. M. Exploration of the Nucleation Pathway for Supramolecular Fibers. *J. Chem. Inf. Model.* **2023**, *63* (8), 2419–2426.

(22) Sis, M. J.; Ye, Z.; La Costa, K.; Webber, M. J. Energy Landscapes of Supramolecular Peptide-Drug Conjugates Directed by Linker Selection and Drug Topology. *ACS Nano* **2022**, *16* (6), 9546–9558.

(23) Nidadavolu, L. S.; Stern, D.; Lin, R.; Wang, Y.; Li, Y.; Wu, Y.; Marin, S.; Antonio, M. J.; Yenokyan, G.; Boronina, T.; Cole, R.; Foster, D. B.; Talbot, C.; Jedrych, J.; Smith, B.; Rini, D.; Le, A.; Cui, H.; Walston, J. D.; Abadir, P. M. Valsartan Nano-Filaments Alter Mitochondrial Energetics and Promote Faster Healing in Diabetic Rat Wounds. *Wound Repair Regen.* **2021**, *29* (6), 927–937.

(24) Chakroun, R. W.; Wang, F.; Lin, R.; Wang, Y.; Su, H.; Pompa, D.; Cui, H. Fine-Tuning the Linear Release Rate of Paclitaxel-Bearing Supramolecular Filament Hydrogels through Molecular Engineering. *ACS Nano* **2019**, *13* (7), 7780–7790.

(25) Bennett, W. F. D.; MacCallum, J. L.; Tieleman, D. P. Thermodynamic Analysis of the Effect of Cholesterol on Dipalmitoylphosphatidylcholine Lipid Membranes. *J. Am. Chem. Soc.* **2009**, *131* (5), 1972–1978.

(26) De Santis, E.; Ryadnov, M. G. Peptide Self-Assembly for Nanomaterials: The Old New Kid on the Block. *Chem. Soc. Rev.* **2015**, *44* (22), 8288–8300.

(27) Batra, R.; Loeffler, T. D.; Chan, H.; Srinivasan, S.; Cui, H.; Korendovych, I. V.; Nanda, V.; Palmer, L. C.; Solomon, L. A.; Fry, H. C.; Sankaranarayanan, S. K. R. S. Machine Learning Overcomes Human Bias in the Discovery of Self-Assembling Peptides. *Nat. Chem.* **2022**, *14* (12), 1427–1435.

(28) Ramakrishnan, M.; van Teijlingen, A.; Tuttle, T.; Ulijn, R. V. Integrating Computation, Experiment, and Machine Learning in the Design of Peptide-Based Supramolecular Materials and Systems. *Angew. Chem. Int. Ed Engl.* **2023**, *62* (18), e202218067.

(29) van Teijlingen, A.; Tuttle, T. Beyond Tripeptides Two-Step Active Machine Learning for Very Large Data Sets. *J. Chem. Theory Comput.* **2021**, *17* (5), 3221–3232.

(30) Zhang, P.; Cheetham, A. G.; Lin, Y.-A.; Cui, H. Self-Assembled Tat Nanofibers as Effective Drug Carrier and Transporter. *ACS Nano* **2013**, *7* (7), 5965–5977.

(31) Sahoo, J. K.; VandenBerg, M. A.; Webber, M. J. Injectable Network Biomaterials via Molecular or Colloidal Self-Assembly. *Adv. Drug Deliv. Rev.* **2018**, *127*, 185–207.

(32) Webber, M. J.; Pashuck, E. T. (Macro)molecular Self-Assembly for Hydrogel Drug Delivery. *Adv. Drug Deliv. Rev.* **2021**, *172*, 275–295.

(33) Pashuck, E. T.; Cui, H.; Stupp, S. I. Tuning Supramolecular Rigidity of Peptide Fibers through Molecular Structure. *J. Am. Chem. Soc.* **2010**, *132* (17), 6041–6046.

(34) Yu, S.; Xian, S.; Ye, Z.; Pramudya, I.; Webber, M. J. Glucose-Fueled Peptide Assembly: Glucagon Delivery via Enzymatic Actuation. *J. Am. Chem. Soc.* **2021**, *143* (32), 12578–12589.

(35) Vedadghavami, A.; Wagner, E. K.; Mehta, S.; He, T.; Zhang, C.; Bajpayee, A. G. Cartilage Penetrating Cationic Peptide Carriers for Applications in Drug Delivery to Avascular Negatively Charged Tissues. *Acta Biomater.* **2019**, *93*, 258–269.

(36) Evans, C. H.; Kraus, V. B.; Setton, L. A. Progress in Intra-Articular Therapy. *Nat. Rev. Rheumatol.* **2014**, *10* (1), 11–22.

(37) Weissleder, R.; Tung, C. H.; Mahmood, U.; Bogdanov, A., Jr. In Vivo Imaging of Tumors with Protease-Activated near-Infrared Fluorescent Probes. *Nat. Biotechnol.* **1999**, *17* (4), 375–378.

(38) Paramonov, S. E.; Jun, H.-W.; Hartgerink, J. D. Self-Assembly of Peptide-Amphiphile Nanofibers: The Roles of Hydrogen Bonding and Amphiphilic Packing. *J. Am. Chem. Soc.* **2006**, *128* (22), 7291–7298.

(39) Marek, P. J.; Patsalo, V.; Green, D. F.; Raleigh, D. P. Ionic Strength Effects on Amyloid Formation by Amylin Are a Complicated Interplay among Debye Screening, Ion Selectivity, and Hofmeister Effects. *Biochemistry* **2012**, *51* (43), 8478–8490.

(40) Wang, H.; Su, H.; Xu, T.; Cui, H. Utilizing the Hofmeister Effect to Induce Hydrogelation of Nonionic Supramolecular Polymers into a Therapeutic Depot. *Angew. Chem. Int. Ed Engl.* **2023**, *62* (43), e202306652.

(41) Synthesis and Chemical Stability of Glucocorticoid-Dextran Esters: Potential Prodrugs for Colon-Specific Delivery. *Int. J. Pharm.* **1993**, *92* (1-3), 105–114.

(42) Bender, D. M.; Peterson, J. A.; McCarthy, J. R.; Gunaydin, H.; Takano, Y.; Houk, K. N. Cyclopropanecarboxylic Acid Esters as Potential Prodrugs with Enhanced Hydrolytic Stability. *Org. Lett.* **2008**, *10* (3), 509–511.

(43) Ma, W.; Su, H.; Cheetham, A. G.; Zhang, W.; Wang, Y.; Kan, Q.; Cui, H. Synergistic Antitumor Activity of a Self-Assembling Camptothecin and Capecitabine Hybrid Prodrug for Improved Efficacy. *J. Control. Release* **2017**, *263*, 102–111.

(44) Cui, H.; Cheetham, A. G.; Pashuck, E. T.; Stupp, S. I. Amino Acid Sequence in Constitutionally Isomeric Tetrapeptide Amphiphiles Dictates Architecture of One-Dimensional Nanostructures. *J. Am. Chem. Soc.* **2014**, *136* (35), 12461–12468.

(45) Zhang, Y.; Zhou, T.; Qi, Y.; Li, Y.; Zhang, Y.; Zhao, Y.; Han, H.; Wang, Y. Engineered Assemblies from Isomeric Pentapeptides Augment Dry Eye Treatment. *J. Control. Release* **2024**, *365*, 521–529.

(46) Tantakitti, F.; Boekhoven, J.; Wang, X.; Kazantsev, R. V.; Yu, T.; Li, J.; Zhuang, E.; Zandi, R.; Ortony, J. H.; Newcomb, C. J.; Palmer, L. C.; Shekhawat, G. S.; de la Cruz, M. O.; Schatz, G. C.; Stupp, S. I. Energy Landscapes and Functions of Supramolecular Systems.

Nat. Mater. **2016**, *15* (4), 469–476.
(47) Ortony, J. H.; Newcomb, C. J.; Matson, J. B.; Palmer, L. C.; Doan, P. E.; Hoffman, B. M.; Stupp, S. I. Internal Dynamics of a Supramolecular Nanofibre. *Nat. Mater.* **2014**, *13* (8), 812–816.
(48) Kriebisch, B. A. K.; Kriebisch, C. M. E.; Bergmann, A. M.; Wanzke, C.; Tena-Solsona, M.; Boekhoven, J. Tuning the Kinetic Trapping in Chemically Fueled Self-Assembly**. *ChemSystemsChem* **2023**, *5* (1), e202200035.
(49) Lakshminarayanan, V.; Chockalingam, C.; Mendes, E.; van Esch, J. H. Gelation Kinetics-Structure Analysis of pH-Triggered Low Molecular Weight Hydrogelators. *Chemphyschem* **2021**, *22* (21), 2256–2261.
(50) Singh, N.; Lainer, B.; Formon, G. J. M.; De Piccoli, S.; Hermans, T. M. Re-Programming Hydrogel Properties Using a Fuel-Driven Reaction Cycle. *J. Am. Chem. Soc.* **2020**, *142* (9), 4083–4087.